Plasma Sources Science and Technology

PAPER • **OPEN ACCESS**

Erosion and cathodic arc plasma of Nb–Al cathodes: composite versus intermetallic

To cite this article: Siegfried Zöhrer *et al* 2020 *Plasma Sources Sci. Technol.* **29** 025022

OPEN ACCESS
IOP Publishing
Plasma Sources Science and Technology
Plasma Sources Sci. Technol. **29** (2020) 025022 (14pp)
https://doi.org/10.1088/1361-6595/ab5e32

Erosion and cathodic arc plasma of Nb–Al cathodes: composite versus intermetallic

Siegfried Zöhrer[1,5], Mehran Golizadeh[1], Nikola Koutná[2,3], David Holec[1], André Anders[4,6,7] and Robert Franz[1]

[1] Department of Materials Science, Montanuniversität Leoben, Leoben, Austria
[2] Institute of Materials Science and Technology, TU Wien, Vienna, Austria
[3] Department of Condensed Matter Physics, Masaryk University, Brno, Czech Republic
[4] Lawrence Berkeley National Laboratory, Berkeley, United States of America

E-mail: szoehrer@alumni.tugraz.at

Received 7 August 2019, revised 25 November 2019
Accepted for publication 3 December 2019
Published 20 February 2020

Abstract

Many properties of cathodic arcs from single-element cathodes show a correlation to the cohesive energy of the cathode material. For example, the burning voltage, the erosion rate, or, to a lesser extent, plasma properties like electron temperatures or average ion energy and charge states. For multi-element cathodes, various phases with different cohesive energies can initially be present in the cathode, or form due to arc exposure, complicating the evaluation of such correlations. To test the influence of morphology and phase composition of multi-element cathodes on cathodic arc properties, a Nb–Al cathode model system was used that includes: pure Nb and Al cathodes; intermetallic Nb_3Al, Nb_2Al and $NbAl_3$ cathodes; and three composite Nb–Al cathodes with atomic ratios corresponding to the stoichiometric ratios of the intermetallic phases. Pulsed cathodic arc plasmas from these cathodes were examined using a mass-per-charge and energy-per-charge analyzer, showing that charge-state-resolved ion energy distributions of plasmas from the intermetallic and corresponding composite cathodes are nearly identical. An examination of converted layers of eroded cathodes using x-ray diffraction and scanning electron microscopy indicates the formation of a surface layer with similar phase composition for intermetallic and their corresponding composite cathode types. The average arc voltages do not follow the trend of cohesive energies of Nb, Al and intermetallic Nb–Al phases, which have been calculated using density functional theory. Possible reasons for this effect are discussed based on the current knowledge of multi-element arc cathodes and their arc plasma available in literature.

Keywords: arc discharge, composite cathode, intermetallic cathode, Nb–Al, cathode erosion, ion energy distribution, converted layer

1. Introduction

Cathodic arcs transform the cathode material into a plasma state, a phenomenon which is often utilized to deposit thin films, but can also serve as an ion source for other applications. Depending on cathode material and background gas pressure, multiply charged ions with velocities in the order of 10^4 ms^{-1} are present in the inter-electrode plasma [1]. For cathodic arcs of single-element cathodes in high vacuum, experimental and calculated data for the arc plasma properties covering most conducting elements in the periodic table is available in literature [2–6]. This includes for example, average burning voltages, electron temperatures, ion charge state distributions (ICSDs), or ion energy and velocity distributions. Concepts like the correlation of the cohesive energy of the cathode material to burning voltage, energy input and erosion rate [7], or the independence

[5] Author to whom any correspondence should be addressed.
[6] Leibniz Institute of Surface Engineering (IOM), Leipzig, Germany.
[7] Felix Bloch Institute, Leipzig University, Leipzig, Germany.

or weak dependence of most likely ion velocities on ion charge state [8] show a good agreement to these experimental data sets.

While the second of these two concepts, the so-called 'velocity rule', seems to be applicable also for multi-element cathodes, where also ions of different masses (elements) show similar most likely ion velocities [9], it is still unclear if the other concept, the so-called 'cohesive energy rule', can be applied to multi-element cathodes. In some reports, cohesive energies of multi-element cathode materials are compared to ion properties of the expanded arc plasma, like average ion charge states and energies [10, 11]. These are, however, also for single-element cathodes, only indirectly related to the cohesive energy of the cathode material and can be significantly influenced by other means, e.g. by element specific ionization potentials, charge exchange collisions of ions with neutral species [12, 13], vacuum chamber geometry and the experimental setup, or by angular distributions [14–16]. Therefore, such experiments should be combined with more direct approaches, like e.g. a comparison of cohesive energies to average arc burning voltages as a function of composition of multi-element cathodes. Such comparisons are, however, only rarely reported in literature and the information available is inconclusive. Furthermore, additionally to the elemental fractions of multi-element cathodes, structure and morphology of such cathodes are likely to influence cathodic arc properties. While several experiments indicate the formation of intermetallic phases in the converted layer of eroded composite cathodes [17–19], experiments which explicitly compare cathodic arcs from a cathode composed of an intermetallic phase to a composite cathode with the same elements and atomic ratio seem to be absent in literature, apart from a recent report by [20] in the context of arc deposition. There, the authors compared two kinds of Ti–Al cathodes with different phase compositions: pure α-Ti and Al phases versus a mixture of intermetallic Ti_3Al and TiAl phases, both with 50 at% Al content. The intermetallic cathode showed larger grain sizes in the converted layer, higher population of macro-particles in the coatings and a slightly higher deposition rate.

In previous works, we used a Nb–Al cathode model system including Nb, Al and three composite Nb–Al cathodes with atomic Nb/Al ratios of 75/25, 67/33 and 25/75 to examine average arc voltages, ion energy/velocity and charge state distributions of related pulsed cathodic arc plasmas in high vacuum and Ar atmosphere using high time resolution [21, 22]. The determined voltages and ion properties of arcs from composite Nb–Al cathodes did, however, not show a simple linear interpolation between their single-element counterparts like e.g. suggested by [23] based on the Ti–Hf system. Particularly, the reason why the average arc voltage of the composite Nb–Al cathode with 25 at% Nb content showed a clearly lower value compared to that of the pure Al cathode is not fully understood. To further elaborate these results and the role of intermetallic phases and cohesive energies for cathodic arcs from multi-element cathodes, we extent our Nb–Al model system with 3 cathodes, where each of them is composed of one intermetallic phase in the Nb–Al system: Nb_3Al, Nb_2Al and $NbAl_3$. Such an extended cathode model system allows us to examine possible influences of cathode phase composition to cathodic arc properties like average arc voltage, ion energy distributions (IEDs),

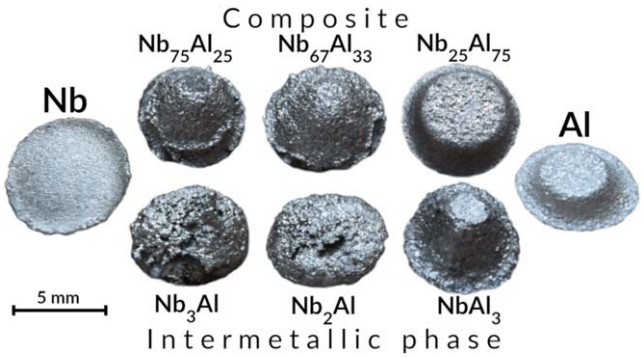

Figure 1. Top surfaces of used cylindrical Nb, Al and Nb–Al cathodes, showing different surface structures due to erosion after approximately 10^4 plasma pulses.

ICSDs and elemental ion fractions in the expanded plasma of pulsed cathodic arcs. In addition, cohesive energies of relevant Nb–Al phases were calculated and the converted layers of eroded cathodes were analyzed using scanning electron microscopy (SEM) and grazing incidence x-ray diffraction (XRD).

2. Methods

2.1. Cathodes

Cylindrical cathodes with a diameter of 6.35 mm and about 20 mm length were fabricated by 'Plansee Composite Materials GmbH' in Lechbruck, Germany. Powders of Nb, Al and intermetallic Nb–Al phases were used to create 8 different cathode materials: Nb, Al, Nb–Al composites with Nb fractions of 25, 67 and 75 at% (referred to as $Nb_{25}Al_{75}$, $Nb_{67}Al_{33}$ and $Nb_{75}Al_{25}$), and 3 intermetallic Nb–Al phases: $NbAl_3$, Nb_2Al and Nb_3Al. An overview of these cathodes is shown in figure 1. The powders had grain sizes smaller than 135 μm and a purity of at least 99.9%. The fabricated cathodes were analyzed using XRD and SEM of fractured surfaces and polished microcuts, as well as by a chemical analysis to determine possible contaminations.

2.2. Arc source and plasma diagnostics

The basic experimental setup is sketched in figure 2 and similar to previous experiments [21, 22]. The cathodes were mounted in an 'arc miniature gun' (described in detail elsewhere [24, 25]) positioned in a vacuum chamber of 1 m diameter and 0.25 m height, which was initially evacuated by a scroll pump and then by a cryogenic pump to a base pressure of 10^{-4} Pa, representing the starting point for all measurements. The cathode cylinder axis was pointing directly towards a grounded 50 μm orifice of a mass-energy-analyzer (MEA, model EQP300 by Hiden) at a distance of about 27 cm, which was differentially pumped to 10^{-6} Pa by a turbomolecular pump. The main elements of the MEA, which are also indicated in figure 2, are: an ion extractor (extr.); an ion drift space followed by an electric sector field energy filter (ESA); a quadrupole mass per charge filter; a secondary electron multiplier (det.); and the mass spectrometer interface

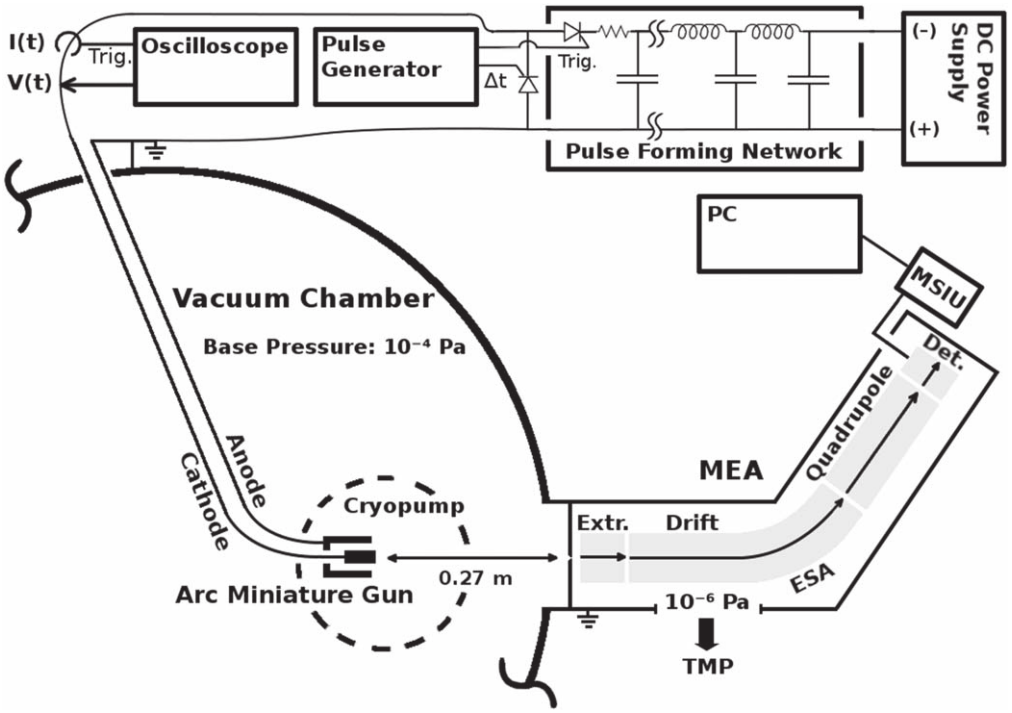

Figure 2. Basic sketch of the experimental setup, indicating the arc miniature gun in the vacuum chamber, the attached mass-energy analyzer (MEA), the electric circuit and other peripheral devices. Further details are explained in the text. This figure was adapted from figure 1 in [21], licensed under Creative Commons Attribution 3.0.

unit. Further details and applied parameters can be found in [21].

To generate arc discharges, a 1 kV power supply was charging a pulse forming network (PFN) with 250 V, delivering an approximately rectangular 200 A current pulse of 1 ms to the arc miniature gun. The pulse was cut-off at 600 μs (which corresponds to Δt in figure 2) by redirecting the current into a short circuit to enhance its rectangular shape. As a consequence of a conducting path between cathode and anode within the arc miniature gun with an electrical resistance between 1 and 500 Ω, the applied voltage is sufficient to trigger an arc discharge (see [25] for details on this trigger mechanism). Arc pulses were generated 5 times per second. Before starting or restarting any measurement, a conditioning step of about 150 arc pulses was generally carried out to ensure arc spots of type 2 [26].

The MEA was used to detect ions of the plasma resolved in mass-per-charge and energy-per-charge. The detection interval (the 'dwell time') was set to 1 s per energy step, which means that each individual measurement is an average of 5 consecutive arc pulses. IEDs have been recorded with a step size of q eV, where q is the charge state number of the related ion species. Based on the natural abundance of $^{27}_{13}$Al (100.0%) and $^{93}_{41}$Nb (100.0%) [27], no isotope corrections were applied. It has to be stressed that these results reflect the situation at the MEA orifice 27 cm away from the cathode at an on-axis angle (normal to the cathode surface) and only provide indirect information on the cathodic arc plasma. The change of kinetic ion energy in the plasma sheath to this grounded orifice was not corrected.

2.3. Arc voltage and current

Voltages and currents of the arc discharge were measured directly at the vacuum chamber feedthrough using a 1:100 high voltage probe and a 0.01 V A^{-1} wide-band current monitor. One has to be aware that these voltages are slightly larger than the actual arc burning voltage, which is a result of the voltage drop inside the cathode and other relevant parts of the circuit. Therefore, they are here, denoted as 'arc voltages' instead of burning voltages. To be able to compare arc voltages of cathodic arcs from intermetallic Nb–Al cathodes to our earlier measurements of composite Nb–Al cathodes in high vacuum, where a nearly identical experimental setup was used, the measurement of voltage samples was done separately and similarly to [21]. That is, recording the time evolution of voltage (and current) averaged over ≈65 plasma pulses several times (≈100 iterations). An exemplary evolution of voltage and current within an arc pulse from a Nb_3Al cathode is displayed in figure 3. A pulse time interval representative for a steady state regime (300–500 μs) was used to compute a final average value of all samples corresponding to one cathode material.

2.4. Characterization of eroded cathodes

After being exposed to roughly 10^4 plasma pulses, the crystallographic structure of the eroded cathode surface layers was examined using grazing incidence XRD with a fixed incident angle of 2°, while the 2θ angle was varied from 10 to 120° with a step size of 0.035° and a dwell time of 2 s. Images of such eroded cathode surface layers are shown in figure 1 for all cathode materials. For these

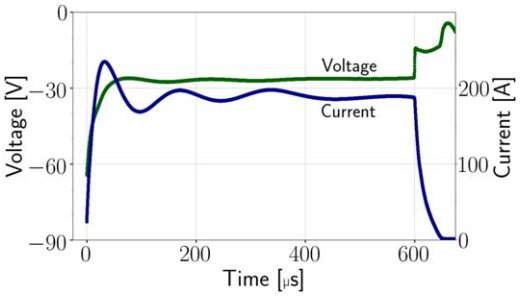

Figure 3. Typical time evolution of voltage and current during an arc pulse, showing results from an Nb_3Al cathode. The arc is triggered at time zero and cut-off at 600 μs. Reproduced from [21]. © IOP Publishing Ltd. All rights reserved.

measurements, a Bruker D8 Advance diffractometer equipped with an energy-dispersive Sol-X detector and CuK_α radiation was used. These measurements were repeated for the virgin cathodes using the same parameters. Cross sections of the eroded cathodes were prepared by grinding and polishing to a finish of 1 μm. These cross sections were analyzed by SEM using a Zeiss EVO 50. Backscattered electron (BSE) images were recorded to visualize the elemental contrast between Nb and Al.

2.5. Approximation of cohesive energies

In order to estimate cohesive energies of relevant Nb, Al and Nb–Al phases, density functional theory (DFT) calculations were performed using the Vienna *Ab initio* Simulation Package [28, 29] together with plane-wave projector augmented wave pseudopotentials [30]. The Perdew–Burke–Ernzerhof generalized gradient approximation (PBE) [31] was used to treat the exchange and correlation effects. The plane-wave cut-off energy of 600 eV and the reciprocal space sampling with Γ-centered Monkhorst–Pack meshes [32] ensured a total energy accuracy of at least 10^{-3} eV per atom. The Nb–Al intermetallics, $NbAl_3$, Nb_2Al, and Nb_3Al, were assumed to adopt the tetragonal DO_{22} ($I4/mmm$, #139), tetragonal $D8_b$ ($P4_2/mnm$, #136), and cubic A15-type ($Pm3n$, #223) phase, respectively. Additionally, low-energy metastable Nb_xAl_{1-x} structures were predicted [33] employing first-principles evolutionary algorithms as implemented in the USPEX (universal Structure Predictor: Evolutionary Xtallography) code [34–36] featuring local optimization, real-space representation and flexible physically motivated variation operators. The cohesive energies (E_{coh}) were evaluated according to

$$-E_{coh} = (E_{tot} - n_{Al}E_{free-Al} - n_{Nb}E_{free-Nb}) \cdot \frac{1}{n_{Al} + n_{Nb}}, \quad (1)$$

where E_{tot} is the total energy of the simulation cell, n_{Al} (n_{Nb}) denotes the number of Al (Nb) atoms within the cell, and $E_{free-Al}$ ($E_{free-Nb}$) represents the energy of an isolated Al (Nb) atom in vacuum. The latter is calculated using a large simulation box (15 Å) to avoid interactions between its periodic images, containing a single atom. These calculations were performed with a single k-point (Γ) to further underline the desired non-periodic character.

3. Results

3.1. Plasma properties

IEDs in the plasmas from composite and intermetallic cathode types are directly compared in figure 4 for Nb ions and in figure 5 for Al ions. In both figures, IEDs for the observed charge states (rows) and the 3 different atomic Nb/Al ratios in the cathode are displayed. Apart from small deviations such as a small shift to lower energies for ions from the intermetallic $NbAl_3$ cathode for single-charged ions, the IEDs for the composite and intermetallic cathode types show a similar behavior for all Nb and Al ions species. The generally observable cathode material dependency of these IEDs is displayed more clearly in figure 6 for plasma from composite cathodes, exemplary for the most prominent ions: Nb^{3+} and Al^{2+}.

The Nb ion fraction (f_{Nb}) of the detected Nb and Al ions was calculated with equation (2) using the energy-integrated IEDs for Nb (I_{Nb^q}) and Al ions (I_{Al^q}) of specific charge state numbers q. The results are visualized in figure 7, which compares the fraction of Nb atoms in the cathodes (25, 67 and 75 at%, green bars) to f_{Nb} from composite (blue bars) and intermetallic cathode types (red bars). The results show a surplus of detected Nb ions, when related to the Nb/Al atom ratio in the composite cathodes similar to [21]. For the intermetallic cathode types, this Nb ion surplus is also present

$$f_{Nb} = \frac{\sum_{q=1}^{4} I_{Nb^q}}{\sum_{q=1}^{4} I_{Nb^q} + \sum_{q=1}^{3} I_{Al^q}}. \quad (2)$$

3.2. Arc voltages and cohesive energies

Average arc voltages representing the steady state of the plasma pulses are displayed in figure 8(a) for single-element Nb and Al, composite Nb–Al and intermetallic Nb–Al cathodes. For the single-element and composite Nb–Al cathodes, 4 repetitions of the measurements described in section 2 are shown (including results from [21]). They are directly compared to a single measurement for intermetallic cathodes, where the error bars indicate standard deviation of the sample data, which can be large due to the intrinsic voltage fluctuations of cathodic arcs [37]. Furthermore, differences induced by cathode mounting, cathode erosion and formation of a metal film on the insulator between cathode and anode during the process, can explain the rather strong variations in the results for a single cathode composition. The voltages of the intermetallic cathodes generally follow the known characteristics of composite Nb–Al cathodes [21, 22], but the voltage of the $NbAl_3$ cathode is clearly increased compared to its composite counterpart.

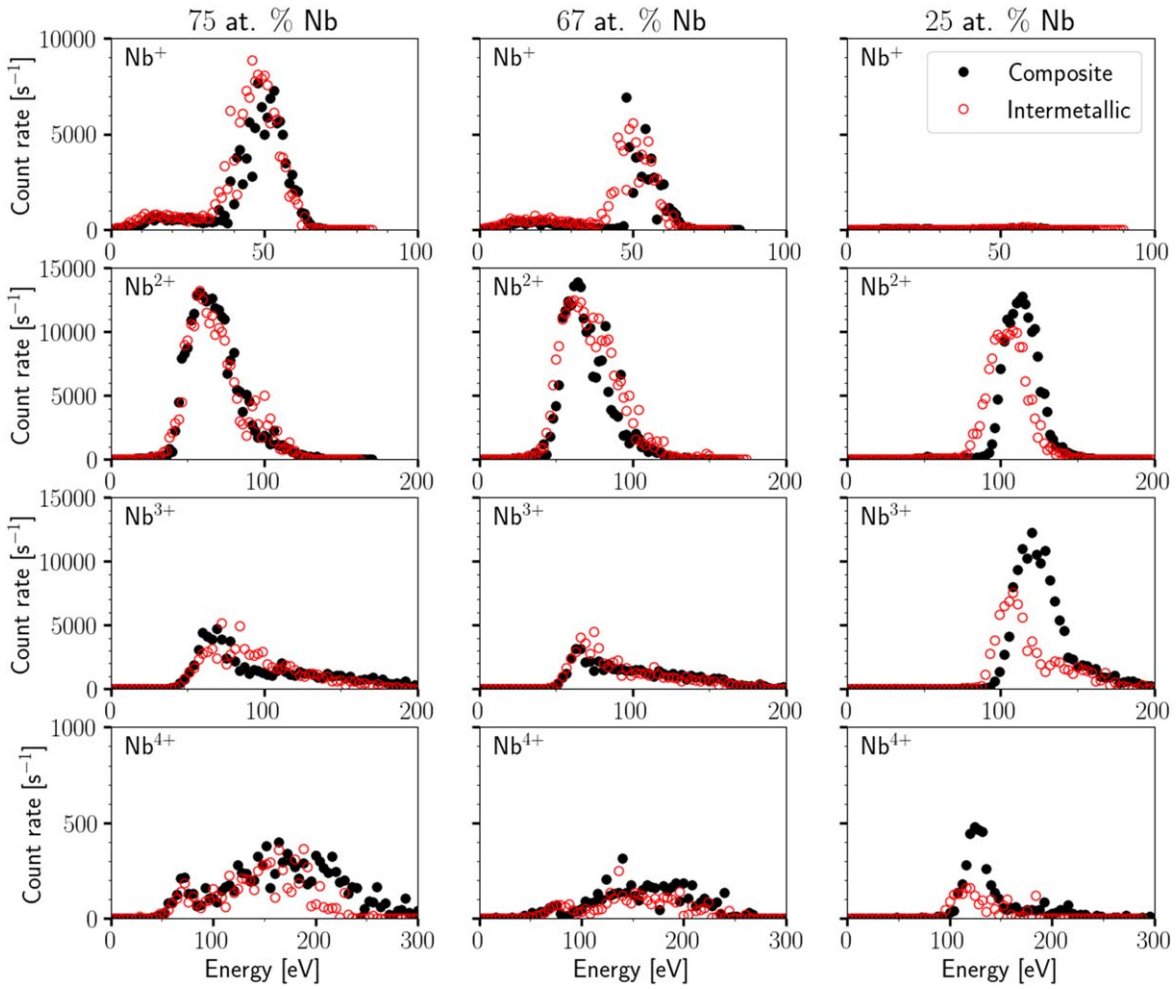

Figure 4. Comparison of Nb IEDs from pulsed cathodic arcs of composite (black markers) and intermetallic (red markers) cathodes. These distributions are displayed for all observed Nb ion charge states (rows) and different Nb contents in the Nb–Al cathodes (columns).

The arc currents are constant for all cathode materials (≈200 A) due to the total impedance being dominated by the PFN and not by the arc discharge.

Figure 8(b) displays the DFT calculated cohesive energies of the cathode materials as well as of the metastable Nb_xAl_{1-x} phases predicted by USPEX. The cohesive energy estimates are compared with experimental data from literature for Nb and Al [38] as well as with other DFT approaches for Nb using different parameters [39]. While the results for Al match the shown literature values, the discrepancies for the Nb values display the general difficulty of calculating cohesive energies of transition metals using DFT, where the choice of approximation of the exchange correlation energy has a particularly large influence [39]. Still, the use of PBE leads to the same result of about 7.0 eV here, as well as in [39]. To achieve comparable results, all cohesive energies in the current work (including fcc-Al and bcc-Nb) were calculated using the same DFT approach as described in section 2. We note that according to 0 K DFT calculations, the only stable structures within the binary Nb–Al system are bcc-Nb, Nb_2Al, $NbAl_3$, and fcc-Al (all marked by red triangles). Nb_3Al, although present in the experiments, is dynamically unstable (even at higher temperatures) and was proposed to be stabilized by antisite defects [33].

3.3. Characterization of eroded cathodes

3.3.1. SEM. Cross-sectional SEM images from used Nb–Al cathodes are displayed in figure 9 for the composite and in figure 10 for the intermetallic cathode types. For the composite cathodes, the bulk material shows Nb powder grains (bright) embedded in an Al matrix (dark) due to the powder metallurgical fabrication process. In addition, the so-called converted layer is clearly noticeable from material contrast in the surface-near region. The detailed views of the converted layer show various material contrasts between the Nb grains due to intermixing of Al and Nb in these regions.

In contrast to the composites, the intermetallic cathodes are single phase, and therefore, show less material contrasts in the BSE images (figure 10). The bright streaks in figure 10(a) possibly show Nb or Nb_2Al inclusions formed during the cathode fabrication process and are also visible in other SEM images from fractured surfaces of $NbAl_3$ cathodes (not shown here). The bright features in figure 10(c) are charging effects and can be neglected. The images also display multiple

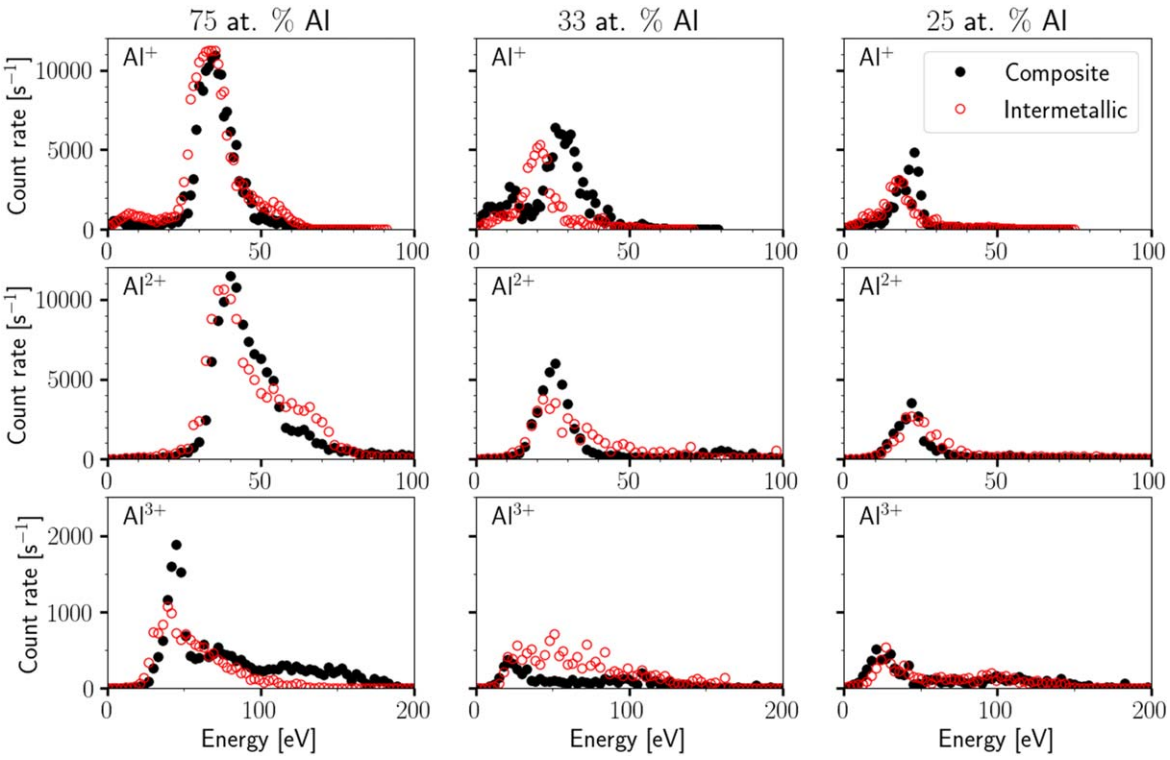

Figure 5. Comparison of Al IEDs from pulsed cathodic arcs of composite (black markers) and intermetallic (red markers) cathodes. These distributions are displayed for all observed Al ion charge states (rows) and different Al contents in the Nb–Al cathodes (columns).

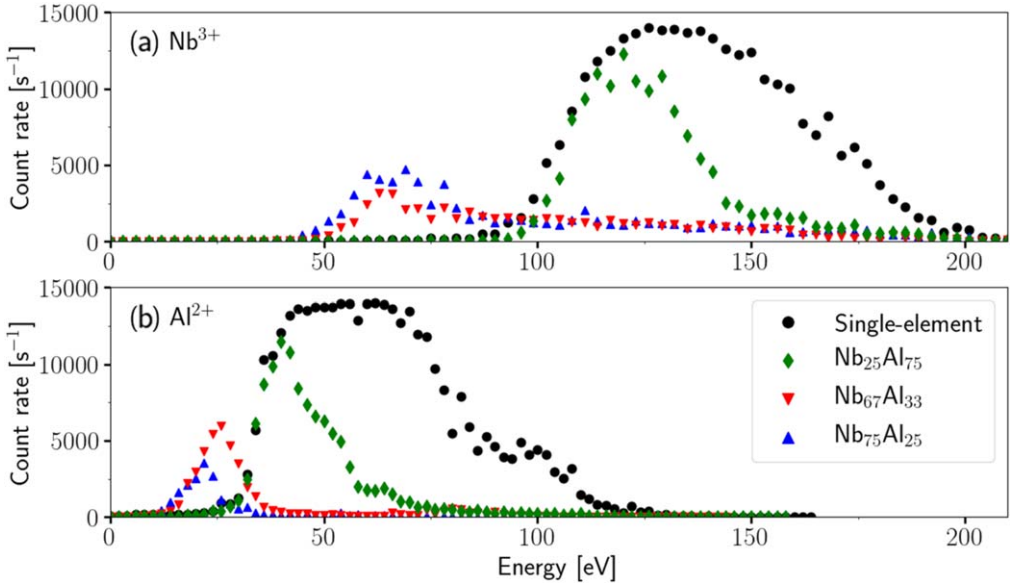

Figure 6. Time-averaged kinetic energy distributions of (a) Nb^{3+} and (b) Al^{2+} ions from cathodic arc plasmas of Nb, Al and composite Nb–Al cathodes.

cracks, related to the generally observed brittleness of the used intermetallic materials. Near the eroded surface, the Nb_2Al and Nb_3Al cathodes show hollow structures (macroscopic flakes partially breaking off). These structures are visible in figures 10(c) and (e) in form of islands within the mounting resin. With incorporation of the detailed views, converted layers are also visible for these intermetallic cathodes in figures 10(b), (d) and (f), particularly for the $NbAl_3$ cathode.

3.3.2. XRD. To determine the phase composition of the converted layers, all cathodes (in virgin and eroded state) were analyzed by XRD. Figure 11 shows the resulting diffractograms for the $Nb_{25}Al_{75}$ and $NbAl_3$ cathodes. The top

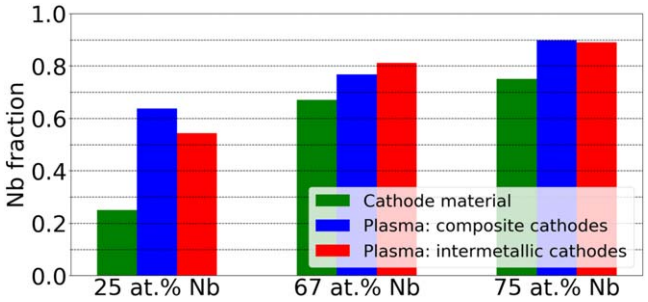

Figure 7. Nb atom fraction in the Nb–Al cathodes (1st bars in green) compared to the Nb ion fraction of the total ion detections from the plasma of composite (2nd bars in blue) and intermetallic (3rd bars in red) cathodes.

(a) and bottom (d) diffractograms in this figure show the results for the virgin cathodes. They are compared to peak patterns taken from literature [40] and clearly display the presence of bcc-Nb and fcc-Al phases (a) and an intermetallic $NbAl_3$ phase (d). For the eroded state (middle), the diffractogram of the eroded intermetallic cathode (c) shows no changes of peak positions. However, the results for the eroded composite cathode (b) indicate the formation of an intermetallic $NbAl_3$ phase at the surface, in addition to bcc-Nb and fcc-Al phases. Additionally, a faint peak at a 2θ angle of 41.2° is appearing (indicated by a thin black line), which is slightly below the highest intensity peak of Nb_2Al according to [40]. Two faint peaks corresponding to the $NbAl_3$ phase are already detected for the virgin composite cathode (also indicated by thin black lines), which is likely caused by the formation of minor amounts of this phase during fabrication.

Figure 12 displays the same type of diagram, but for the $Nb_{67}Al_{33}$ and Nb_2Al cathodes. The diffractogram for the virgin Nb_2Al cathode at the bottom (d) corresponds to calculated peak patterns of an intermetallic Nb_2Al phase obtained from [40]. One additional peak (indicated by a thin black line) near the highest intensity Nb peak (slightly shifted) is also visible. The diffractogram for the eroded state of the Nb_2Al cathode (c) shows a similar behavior apart from the peak at a 2θ angle of 39.2° (also indicated by a thin black line), which seems to be superimposed by a peak not present in virgin state. The change from virgin to eroded state for the composite cathodes (figures 12 (a) and (b)) displays a change from Nb and Al to Nb, Al and a $NbAl_3$ phase. Additionally, the assumed Nb_2Al peak at a 2θ angle of 41.2° (which was also visible in figure 11(b) at lower intensity) is appearing in the eroded state (b).

The last diagram, showing the results for the $Nb_{75}Al_{25}$ and Nb_3Al cathodes, is displayed in figure 13. There, the diffractograms of the virgin cathodes ((a) and (d)) also show the expected Nb, Al, or Nb_3Al peaks when compared to reference data [40]. For the virgin intermetallic case (d), two unidentified faint peaks at 37.1° and 38.1° are present, possibly traces of Nb_2Al or other contaminations. In this diagram, also the results for the eroded intermetallic cathode (c) show a substantial change when compared to the virgin state. In eroded state, only 3 peaks are visible within the shown interval while most Nb_3Al peaks are absent. These 3 peaks (and 2 more at higher diffraction angles not shown here) could actually be shifted Nb peaks. The diffractogram of the eroded composite cathode (b) also shows, similar to figures 11(b) and 12(b), significant changes when compared to its virgin state and displays traces of Nb, Al and $NbAl_3$ phases. Peaks of the Nb_2Al phase are only partly present and Nb_3Al peaks are absent (apart from a barely visible shoulder at its highest intensity peak at 38.8°).

4. Discussion

4.1. Plasma

For the discussion of the recorded properties of pulsed cathodic arc plasmas of composite and intermetallic Nb–Al cathodes, the conclusions of earlier experiments have to be taken into account first. Using a similar experimental setup, charge state dependent Nb and Al IEDs of plasma from Nb, Al and composite Nb–Al cathodes have already been recorded in high vacuum with high time resolution [21]. There, the composite $Nb_{75}Al_{25}$ and $Nb_{67}Al_{33}$ cathodes produced similar results, while the results from the composite $Nb_{25}Al_{75}$ cathode differed as generally higher ion energies and charge states in the steady state regime of the plasma pulses were observed. This behavior shows that increasing the Nb content in an Nb–Al cathode does not necessarily lead to higher charge states and kinetic energies of ions in the expanded arc plasma. One reason for that is the interaction of ions with neutral species, which is particularly strong when using the Nb-rich composite cathodes. This heavily decreases the initially higher charge states and energies of ions coming from Nb-rich composite cathodes, significantly contributing to the observed steady state values [21]. The IEDs shown in the current experiment (black lines in figures 4 and 5) represent another measurement using such composite cathodes, which generally show an outcome consistent to the earlier experiments when compared to their time-average over the full pulse duration, e.g. in figure 7 of [21]. The results of the intermetallic Nb–Al cathodes (red lines in figures 4 and 5) are very similar to the results for the composite cathodes, showing the same characteristics like the low kinetic energies for ions coming from Nb-rich composite cathodes. Although there are small differences, mainly for the $NbAl_3/Nb_{25}Al_{75}$ cathodes, which are also present for arc voltages (see figure 8(a)) and to a lesser extent, for Nb ion fractions (see figure 7), the results as a whole suggest that such a change in the structure of the bulk cathode (composite/intermetallic phase with same atomic Nb/Al ratio) has no major consequences for the properties of the expanded arc plasma from Nb–Al cathodes.

4.2. Cathode erosion

To further discuss these results, one has to take the modifications of the cathode surface layer during the arc pulses into account. The analysis of cathodic arc plasmas is generally done after conditioning the cathode surface to establish stable conditions

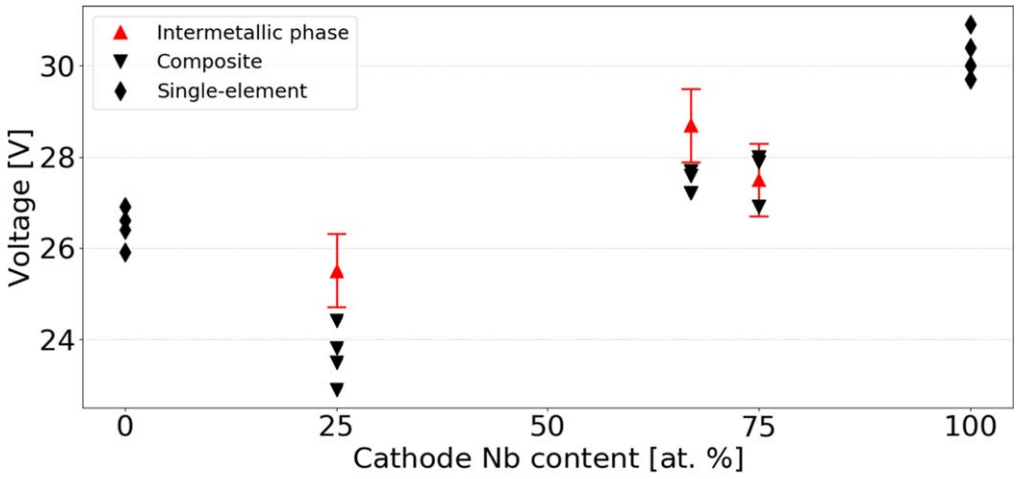

(a) Arc voltages

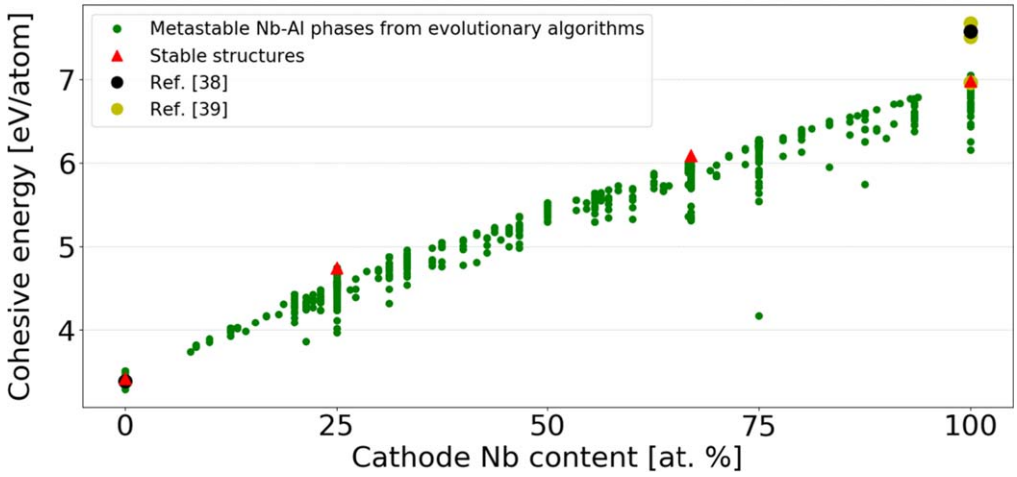

(b) Cohesive energies

Figure 8. (a) Shows average arc voltages of a representative arc pulse time interval for all cathode materials corresponding to the Nb content in the cathode. The black markers show 4 repetitions of measurements for single-element and composite cathodes (where one was taken from table 3 in [21]) and the red markers display results from a single measurement based on intermetallic cathodes, where the error bars represent the voltage fluctuations; (b) displays calculated cohesive energies of Nb, Al and Nb–Al structures from this work and from literature [38, 39]. In addition, cohesive energies of Nb–Al phases predicted by USPEX are shown.

for experiments. That means running the arc discharge before measurements for an adequate amount of time (about 150 arc pulses here) to exclude the influence of various non-metal species initially present on the cathode surface in high vacuum (e.g. oxides or water). When this is done one can expect to have cathode spots of type 2 [26]. This conditioning step, however, already leads to the formation of an converted layer on the cathode before actual measurements are carried out, because the explosive plasma formation within arc spots involves temperatures exceeding the critical point of related phases and might exhibit pressures up to 10^{10} Pa [41, 42]. Consequently, also the still solid or liquid phases in the vicinity of arc spots are likely to undergo phase transitions. The resulting converted layers can be clearly observed in the SEM images for the composite cathodes (figure 9), similarly to other reports in literature for e.g. composite Ti–Al [18] or composite Cr–Al cathode materials [17]. The material contrasts within these layers, suggest the presence of Nb–Al phases (possibly intermetallic or solid solutions) in addition to Nb and Al. When considering the results for the intermetallic cathodes, the layers show less material contrast, but still, converted layers are partly visible (see figure 10), indicating differences in microstructure in the heat-affected zone. Based on these observations, the formation of a similar mixture of phases in the surface layers of the composite and corresponding intermetallic cathodes could be a reason for the observed conformity of related ion properties.

These hypotheses are strengthened by the results of XRD. There, with exception of the eroded Nb_3Al cathode, the diffractograms of all eroded cathodes show traces of the intermetallic $NbAl_3$ and Nb_2Al phases. A mixture of these 2 phases and remainders of the bulk cathode material might be generally present on the eroded cathode surfaces. In the

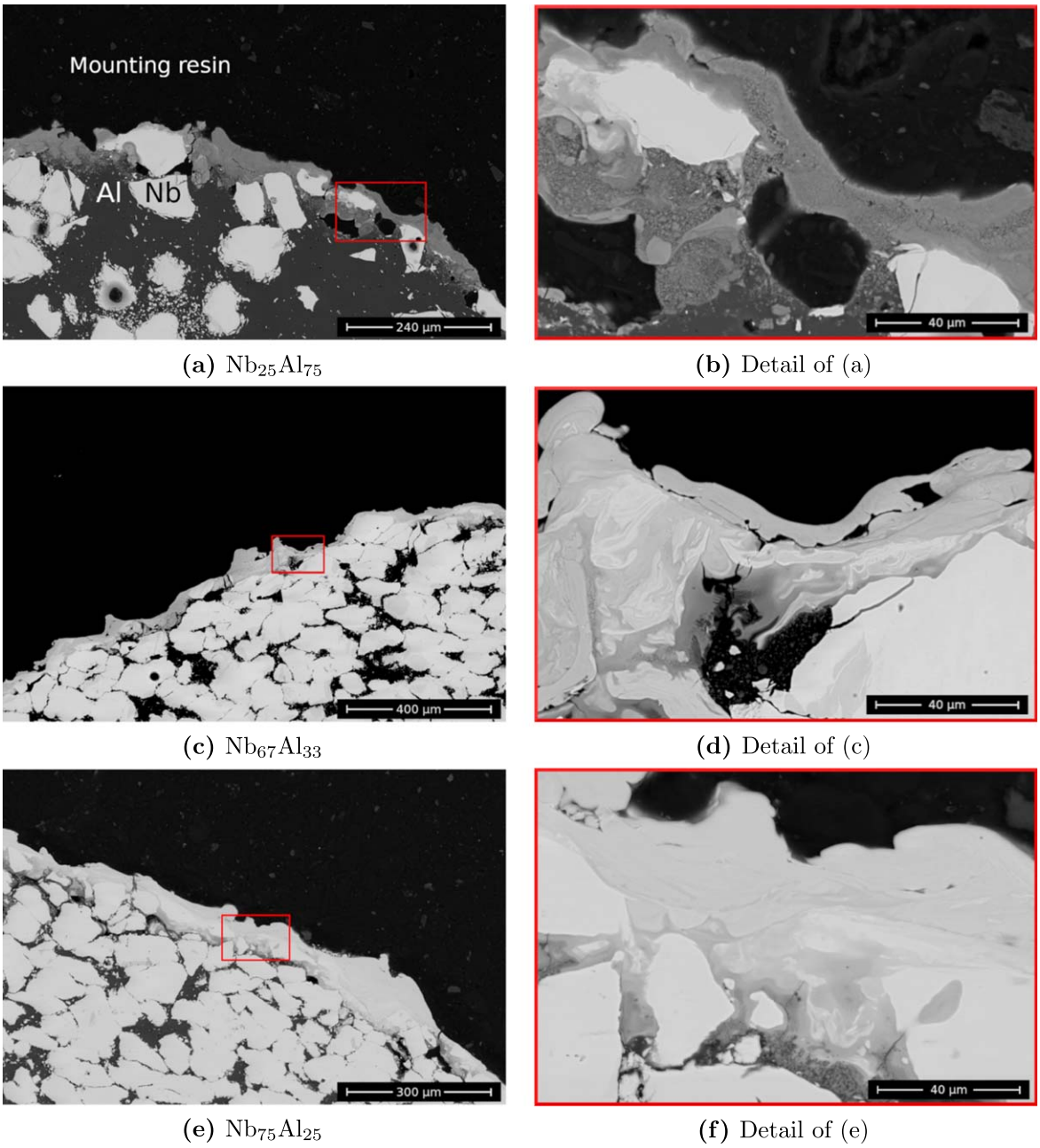

(a) $Nb_{25}Al_{75}$ **(b)** Detail of (a)

(c) $Nb_{67}Al_{33}$ **(d)** Detail of (c)

(e) $Nb_{75}Al_{25}$ **(f)** Detail of (e)

Figure 9. Cross-sectional SEM images of eroded cathodes for composite $Nb_{25}Al_{75}$ (a) + (b), $Nb_{67}Al_{33}$ (c) + (d) and $Nb_{75}Al_{25}$ (e) + (f) materials.

Nb–Al phase diagram (e.g. in an experimentally determined phase diagram shown in [43, 44]) the miscibility gap between the $NbAl_3$ and Nb_2Al phases ranges from about 35 to 75 at% Al at 1000 °C, generally providing a large interval for the formation of these two phases in thermodynamic equilibrium. Considering the high temperatures and temperature gradients near arc spots, it is clear that high cooling rates are likely to lead to rapid solidification far from thermodynamic equilibrium, possibly providing an even stronger driving force for the formation of different phases. Furthermore, diffusion and the powder grain structure of composite cathodes itself create atomic Nb–Al ratios which are locally different to that of the bulk cathode. It is also known that liquid metal is rapidly displaced on the surface at arc spots within time scales of nanoseconds, where liquid metal droplets can gain velocities of several 100 ms^{-1} [45]. As a consequence of all these aspects, the intermetallic phases forming on the eroded surface do not necessarily correspond to the Nb–Al ratio of the bulk cathode. The prevalence of the $NbAl_3$ phase shown in XRD implies that the corresponding exothermic reaction, the formation of $NbAl_3$ out of Nb and Al, is taking place during arc discharges near arc spots, where thermal energy provides the necessary activation energy. Of the 3 intermetallic phases, $NbAl_3$ shows the lowest enthalpy of formation (most negative value) [44, 46, 47]. The latter was experimentally evaluated to (-49 ± 1) kJ mol^{-1} by [44], to (-41 ± 1) kJ mol^{-1} by [46],

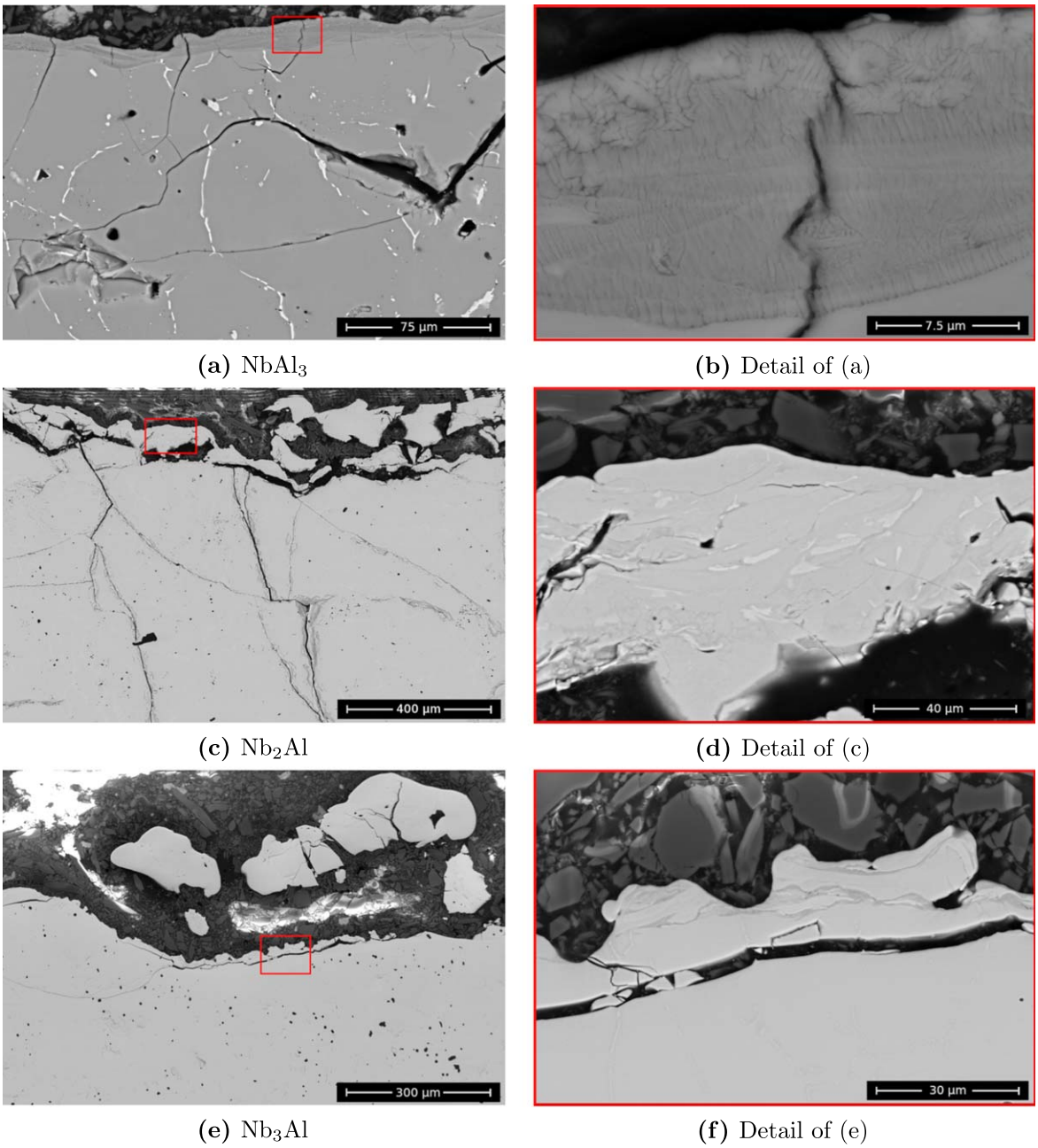

(a) $NbAl_3$ **(b)** Detail of (a)

(c) Nb_2Al **(d)** Detail of (c)

(e) Nb_3Al **(f)** Detail of (e)

Figure 10. Cross-sectional SEM images of eroded intermetallic cathodes: $NbAl_3$ (a) + (b), Nb_2Al (c) + (d) and Nb_3Al (e) + (f).

but also estimated to -46 kJ mol^{-1} by [47] using theoretical approaches. That roughly corresponds to 0.5 eV/atom—similar to calculations in [33]. A locally sufficient supply of Al via diffusion, including the distribution of liquid Al, seems to make this reaction possible, even for lower Al fractions of 25 and 33 at% in the bulk cathode. Similar aspects were discussed by [18] for the Ti–Al system, who examined the erosion of composite $Ti_{50}Al_{50}$ cathodes by cathodic arcs for different Ti/Al grain sizes in the cathode. There, the authors argued that an exothermic reaction for Ti and Al could take place along Al channels in between the Ti grains, which is related to observed porosity and holes beneath the surface. Such porosity in form of holes and cavities, extending up to 100 μm, was also observed for the current eroded Nb–Al cathodes. These cavities could, however, also be related to molten Al beneath the surface, being spilled out due to its thermal expansion. Irrespective of these details, the presence of such exothermic reactions is likely and they might play a role in the energy balance of the cathodic arc discharge.

4.3. Energy balance versus plasma properties

To carry out that thought, a more defining energy for cathodic arcs, the cohesive energy of the cathode material, has to be considered. For single-element cathodes, the approximately linear relationship between arc voltage and cohesive energy of the cathode material is an experimentally well established correlation [7, 48]. When extending that concept to composite

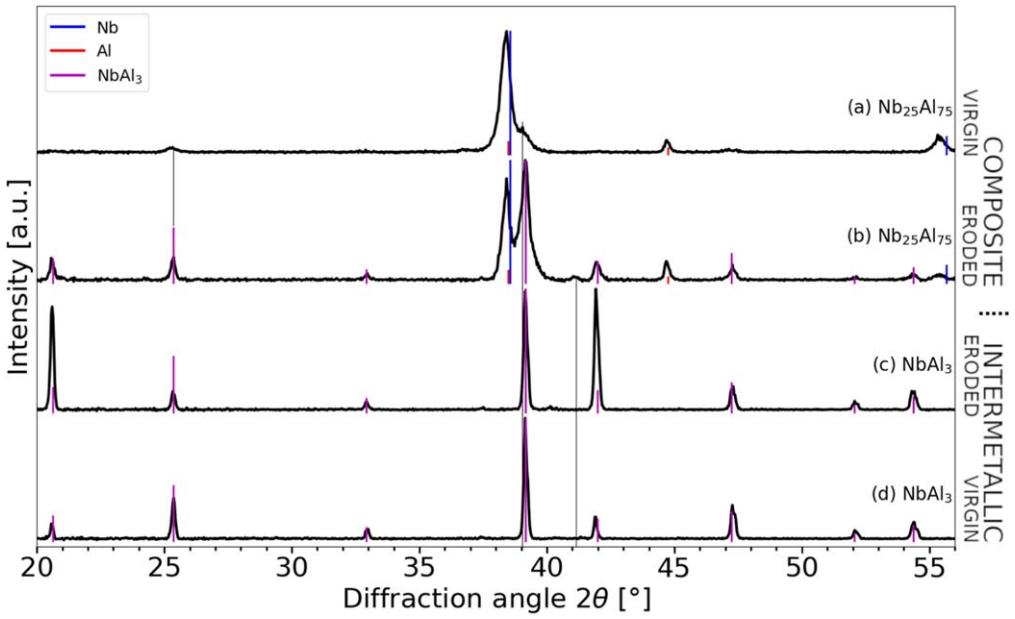

Figure 11. X-ray diffractograms of $Nb_{25}Al_{75}$ and $NbAl_3$ cathodes in virgin and eroded state. The colored peak patterns show literature reference data [40] for bcc-Nb, fcc-Al and $NbAl_3$ phases.

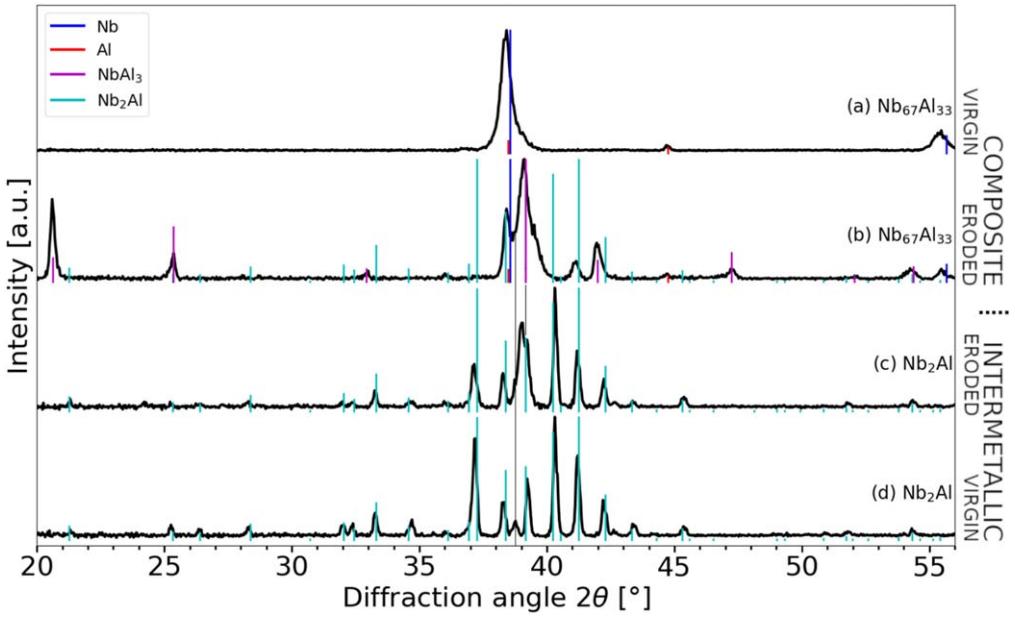

Figure 12. X-ray diffractograms of $Nb_{67}Al_{33}$ and Nb_2Al cathodes in virgin and eroded state. The colored peak patterns show literature reference data [40] for bcc-Nb, fcc-Al, $NbAl_3$ and Nb_2Al phases.

Nb–Al cathodes containing Nb and Al phases, one could simply calculate an average of the cohesive energies of these materials, weighted by the Nb–Al fraction in the cathode. However, since intermetallic Nb–Al phases are present, it is also necessary to consider their cohesive energies, which might show different values. Therefore, DFT was applied to approximate the corresponding average cohesive energies per atom for relevant crystal structures (figure 8(b)). Based on the cohesive energy rule and the results of both of these approaches, which basically show an approximately linear interpolation between the values of Nb and Al, one would expect likewise behavior for the arc voltage. That is, however, not observed (see figure 8(a)) and the measured voltages for the multi-element Nb–Al cathodes are generally lower than predicted by these trends. Since the current is relatively constant for all cathode materials (about 200 A in the steady state regime), the voltage can be easily correlated to power and energy input to the cathode during the steady state regime. The observation that the arc for the composite $Nb_{25}Al_{75}$ cathode requires the least voltage (and power), even

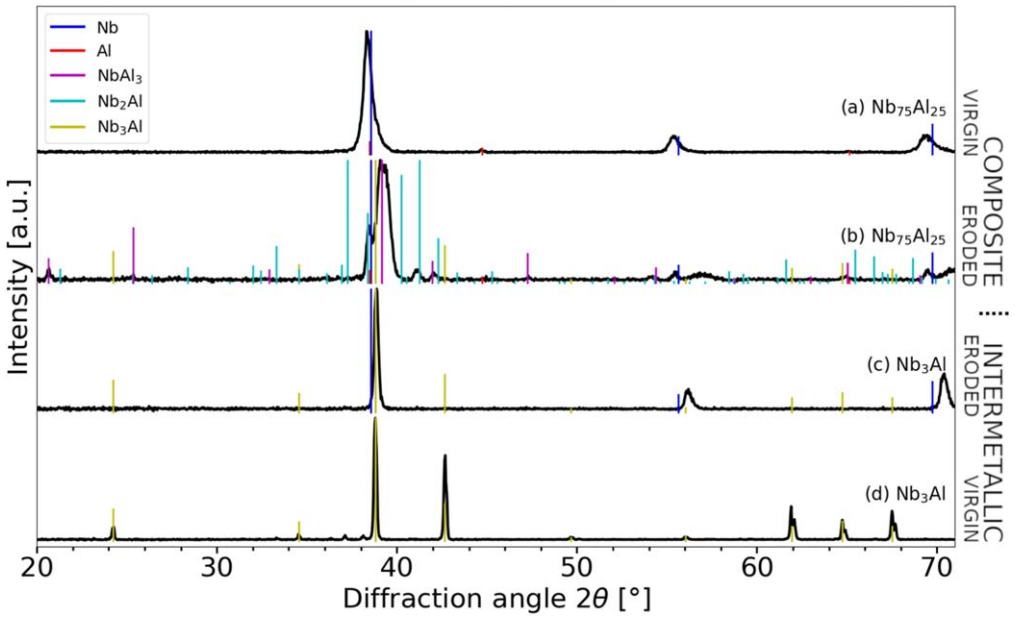

Figure 13. X-ray diffractograms of $Nb_{75}Al_{25}$ and Nb_3Al cathodes in virgin and eroded state. The colored peak patterns show literature reference data [40] for bcc-Nb, fcc-Al, Nb_3Al, Nb_2Al and $NbAl_3$ phases.

Table 1. Melting points (T_m) of Nb and Al [27], and intermetallic Nb–Al phases in their stoichiometric composition (according to [43]).

	Nb	Nb_3Al	Nb_2Al	$NbAl_3$	Al
T_m (°C)	2477	2060	1940	1680	630

less than for the pure Al cathode, cannot be explained by related cohesive energies and is likely caused by other effects.

The exothermic reactions forming the intermetallic phases mentioned earlier could be one of these effects, possibly lowering the energy requirements to sustain the arc due to the provided thermal energy. For the composite cathodes, a steady supply of the reactants Nb and Al is available in form of their body-centered-cubic and face-centered-cubic phases from the bulk cathode. For the intermetallic cathodes however, Nb and Al are only available in form of an intermetallic phase with a much higher melting point compared to Al (see table 1).

The absence of a phase with a low melting and evaporation point like Al in the bulk cathode possibly hinders these reactions and might increase the energy requirements for the arc. That could lead to the observed increase in voltage (and power) for intermetallic cathode types with 25 and 67 at% Nb when compared to the corresponding composite types. The observation that the eroded composite cathodes show pronounced traces of $NbAl_3$ in the diffractograms, while the eroded intermetallic Nb_2Al and Nb_3Al cathodes show less, supports this idea. For the Nb_3Al cathode, where XRD data suggests that even the source material Nb_3Al might not be present in the surface layer, the observed bcc phase with peaks shifted to higher angles than the reference bcc-Nb is most likely a metastable Nb–Al solid solution with the same composition as Nb_3Al.

5. Conclusions

Charge-state-resolved Nb and Al IEDs from pulsed cathodic arc plasmas of intermetallic $NbAl_3$, Nb_2Al and Nb_3Al cathodes were nearly identical to those measured for composite Nb–Al cathodes with corresponding atomic Nb/Al ratios. The formation of a converted layer with a similar phase mixture in heat-affected zones during operation, as indicated by XRD and SEM analysis of the eroded cathodes, seems to be responsible for this behavior. The average arc voltages from intermetallic/composite Nb–Al cathode types also show similar trends, however, the arc voltages of intermetallic cathodes with higher atomic Al fractions are increased. When comparing these voltages to corresponding cohesive energies of relevant phases depending on the atomic Nb/Al ratio in the cathode, no correlation is observed. The measured average arc voltages are lower than expected by a hypothetical extension of the cohesive energy rule to multi-element cathodes. One reason for this deviation could be an altered energy balance of the arc discharge for composite cathodes with high Al content due to the exothermic reaction of elementary Al and Nb forming intermetallic $NbAl_3$ and Nb_2Al phases. Overall, the results demonstrate that for multi-element cathodes like Nb–Al, the converted layer, its phase composition and formation processes play a much more defining role for cathodic arc properties than for single-element cathodes.

Acknowledgments

This work was supported by the Austrian Science Fund (FWF, Project No. P 27867-N36). Work at LBNL was supported by the U.S. Department of Energy under Contract No. DE-AC02-05CH11231. The authors would like to thank

Szilard Kolozsvari and Peter Polcik from Plansee Composite Materials GmbH for their support in cathode fabrication. The computational results presented have been achieved using the Vienna Scientific Cluster (VSC).

ORCID iDs

Siegfried Zöhrer https://orcid.org/0000-0003-2866-6237
Mehran Golizadeh https://orcid.org/0000-0002-0916-8681
David Holec https://orcid.org/0000-0002-3516-1061
André Anders https://orcid.org/0000-0002-5313-6505
Robert Franz https://orcid.org/0000-0003-4842-7276

References

[1] Anders A 2012 The evolution of ion charge states in cathodic vacuum arc plasmas: a review *Plasma Sources Sci. Technol.* **21** 035014
[2] Brown I G 1994 Vacuum arc ion sources *Rev. Sci. Instrum.* **65** 3061–81
[3] Anders A 1997 Ion charge state distributions of vacuum arc plasmas: the origin of species *Phys. Rev.* E **55** 969
[4] Yushkov G Y, Anders A, Oks E M and Brown I G 2000 Ion velocities in vacuum arc plasmas *J. Appl. Phys.* **88** 5618–22
[5] Anders A and Yushkov G Y 2002 Ion flux from vacuum arc cathode spots in the absence and presence of a magnetic field *J. Appl. Phys.* **91** 4824–32
[6] Byon E and Anders A 2003 Ion energy distribution functions of vacuum arc plasmas *J. Appl. Phys.* **93** 1899–906
[7] Anders A, Yotsombat B and Binder R 2001 Correlation between cathode properties, burning voltage, and plasma parameters of vacuum arcs *J. Appl. Phys.* **89** 7764–71
[8] Bugaev A S, Gushenets V I, Nikolaev A G, Oks E M and Yushkov G Y 2000 Study of directed ion velocities in a vacuum arc by an emission method *Tech. Phys.* **45** 1135–40
[9] Zhirkov I, Eriksson A O and Rosén J 2013 Ion velocities in direct current arc plasma generated from compound cathodes *J. Appl. Phys.* **114** 213302
[10] Eriksson A O, Zhirkov I, Dahlqvist M, Jensen J, Hultman L and Rosen J 2013 Characterization of plasma chemistry and ion energy in cathodic arc plasma from Ti–Si cathodes of different compositions *J. Appl. Phys.* **113** 163304
[11] Zhirkov I, Eriksson A, Petruhins A, Dahlqvist M, Ingason A S and Rosén J 2014 Effect of Ti–Al cathode composition on plasma generation and plasma transport in direct current vacuum arc *J. Appl. Phys.* **115** 123301
[12] Anders A, Oks E M and Yushkov G Y 2007 Production of neutrals and their effects on the ion charge states in cathodic vacuum arc plasmas *J. Appl. Phys.* **102** 043303
[13] Anders A and Yushkov G Y 2007 Puzzling differences in bismuth and lead plasmas: evidence for the significant role of neutrals in cathodic vacuum arcs *Appl. Phys. Lett.* **91** 091502
[14] Nikolaev A G, Oks E M, Savkin K P, Yushkov G Y, Frolova V P and Barengolts S A 2014 Charge state, angular distribution, and kinetic energy of ions from multicomponent-cathodes in vacuum arc devices *J. Appl. Phys.* **116** 213303
[15] Nikolaev A G, Savkin K P, Yushkov G Y and Oks E M 2014 Ion angular distribution in plasma of vacuum arc ion source with composite cathode and elevated gas pressure *Rev. Sci. Instrum.* **85** 02B501
[16] Nikolaev A G, Yushkov G Y, Savkin K P and Oks E M 2012 Angular distribution of plasma in the vacuum arc ion source *Rev. Sci. Instrum.* **83** 02A503
[17] Franz R, Martin F M, Hawranek G and Polcik P 2016 Erosion behavior of composite Al–Cr cathodes in cathodic arc plasmas in inert and reactive atmospheres *J. Vac. Sci. Technol.* A **34** 021304
[18] Syed B, Zhu J, Polcik P, Kolozsvari S, Håkansson G, Johnson L, Ahlgren M, Jöesaar M and Odén M 2017 Morphology and microstructure evolution of Ti-50 at% Al cathodes during cathodic arc deposition of Ti–Al–N coatings *J. Appl. Phys.* **121** 245309
[19] Pohler M, Franz R, Ramm J, Polcik P and Mitterer C 2011 Cathodic arc deposition of (Al, Cr)$_2$O$_3$: macroparticles and cathode surface modifications *Surf. Coat. Technol.* **206** 1454–60
[20] Syed B, Jöesaar M J, Polcik P, Kolozsvari S, Håkansson G, Johnson L, Ahlgren M and Odén M 2019 Effect of work function and cohesive energy of the constituent phases of Ti-50 at% Al cathode during arc deposition of Ti–Al–N coatings *Surf. Coat. Technol.* **357** 393–401
[21] Zöhrer S, Anders A and Franz R 2018 Time-resolved ion energy and charge state distributions in pulsed cathodic arc plasmas of Nb–Al cathodes in high vacuum *Plasma Sources Sci. Technol.* **27** 055007
[22] Zöhrer S, Anders A and Franz R 2019 Influence of ar gas pressure on ion energy and charge state distributions in pulsed cathodic arc plasmas from Nb–Al cathodes studied with high time resolution *J. Phys. D: Appl. Phys.* **52** 055201
[23] Sasaki J, Sugiyama K, Yao X and Brown I G 1993 Multiple-species ion beams from titanium–hafnium alloy cathodes in vacuum arc plasmas *J. Appl. Phys.* **73** 7184–7
[24] MacGill R A, Dickinson M R, Anders A, Monteiro O R and Brown I G 1998 Streaming metal plasma generation by vacuum arc plasma guns *Rev. Sci. Instrum.* **69** 801–3
[25] Anders A, Brown I G, MacGill R A and Dickinson M R 1998 Triggerless' triggering of vacuum arcs *J. Phys. D: Appl. Phys.* **31** 584
[26] Lyubimov G A and Rakhovskiĭ V I 1978 The cathode spot of a vacuum arc *Sov. Phys.—Usp.* **21** 693
[27] Lide D R (ed) 2008 *CRC Handbook of Chemistry and Physics* 89th edn (Boca Raton, FL: CRC Press)
[28] Kresse G and Furthmüller J 1996 Efficient iterative schemes for *ab initio* total-energy calculations using a plane-wave basis set *Phys. Rev.* B **54** 11169–86
[29] Kresse G and Joubert D 1999 From ultrasoft pseudopotentials to the projector augmented-wave method *Phys. Rev.* B **59** 1758–75
[30] Kohn W and Sham L J 1965 Self-consistent equations including exchange and correlation effects *Phys. Rev.* **140** A1133–8
[31] Perdew J P, Burke K and Ernzerhof M 1996 Generalized Gradient approximation made simple *Phys. Rev. Lett.* **77** 3865–8
[32] Monkhorst H J and Pack J D 1976 Special points for Brillouin-zone integrations *Phys. Rev.* B **13** 5188
[33] Koutná N, Erdely P, Zöhrer S, Franz R, Du Y, Liu S, Mayrhofer P H and Holec D 2019 Experimental chemistry and structural stability of $AlNb_3$ enabled by antisite defects formation *Materials* **12** 1104
[34] Oganov A R and Glass C W 2006 Crystal structure prediction using *ab initio* evolutionary techniques principles and applications *J. Chem. Phys.* **124** 244704
[35] Lyakhov A O, Oganov A R, Stokes H T and Zhu Q 2013 New developments in evolutionary structure prediction algorithm USPEX *Comput. Phys. Commun.* **184** 1172–82
[36] Oganov A R, Lyakhov A O and Valle M 2011 How evolutionary crystal structure prediction works-and why *Acc. Chem. Res.* **44** 227–37
[37] Anders A 2005 The fractal nature of vacuum arc cathode spots *IEEE Trans. Plasma Sci.* **33** 1456–64

[38] Kittel C 2005 *Introduction to Solid State Physics* 8th edn (New York: Wiley)
[39] Schimka L, Gaudoin R, Klimes J, Marsman M and Kresse G 2013 Lattice constants and cohesive energies of alkali, alkaline-earth, and transition metals: random phase approximation and density functional theory results *Phys. Rev.* B **87** 214102
[40] Gates-Rector S D and Blanton T N 2019 The Powder Diffraction File: a quality materials characterization database *Powder Diffr.* **34** 352–60 Card Numbers: 01-077-3014 (Nb), 00-004-0787 (Al), 03-065-2666 ($NbAl_3$), 01-075-6536 (Nb_2Al), 03-065-4923 (Nb_3Al).
[41] Anders A, Anders S, Forster A and Brown I G 1992 Pressure ionization: its role in metal vapour vacuum arc plasmas and ion sources *Plasma Sources Sci. Technol.* **1** 263
[42] Utsumi T 1971 Measurement of cathode spot temperature in vacuum arcs *Appl. Phys. Lett.* **18** 218–20
[43] Massalski T B *et al* (ed) 1990 *Binary Alloy Phase Diagrams* 2nd edn (Materials Park, OH: ASM International)
[44] Mahdouk K, Gachon J-C and Bouirden L 1998 Enthalpies of formation of the Al–Nb intermetallic compounds *J. Alloys Compd.* **268** 118–21
[45] Boxman R L, Sanders D M and Lafferty P M (ed) 1995 *Handbook of Vacuum Arc Science and Technology* (Park Ridge, NJ: Noyes Publications)
[46] Meschel S and Kleppa O 1993 Standard enthalpies of formation of 4d aluminides by direct synthesis calorimetry *J. Alloys Compd.* **191** 111–6
[47] Papadimitriou I, Utton C and Tsakiropoulos P 2015 *Ab initio* investigation of the Nb–Al system *Comput. Mater. Sci.* **107** 116–21
[48] Anders A, Oks E M and Yushkov G Y 2005 Cathodic arcs: fractal voltage and cohesive energy rule *Appl. Phys. Lett.* **86** 211503